Optical and Quantum Electronics (2023) 55:253
https://doi.org/10.1007/s11082-022-04527-5

THz range natural modes and scattering resonances of circular dielectric micro-cylinder covered with graphene: the H-polarization case

Alexander Ye. Svezhentsev[1] · Alexander I. Nosich[1] · Vladimir Volski[2] · Guy A. E. Vandenbosch[2]

Received: 19 October 2022 / Accepted: 24 December 2022
© The Author(s), under exclusive licence to Springer Science+Business Media, LLC, part of Springer Nature 2023

Abstract
The natural modes (eigenmodes) of graphene-covered circular dielectric micro-cylinders are studied based on the corresponding full-wave electromagnetic eigenvalue problem, in which complex resonance frequencies and corresponding fields are determined numerically. It is shown that the set of complex frequencies splits into two families. The first one corresponds to the modes of the dielectric cylinder perturbed by the graphene cover and the second family represents modes of the graphene cover itself which are plasmon modes. By introducing a transition coefficient, the transformation of the natural modes of the bare dielectric cylinder to the modes of the graphene and the perfectly electric conducting cylinder filled with dielectric are traced. In particular it was shown that the plasmon modes appear not only as a result of the transformation of the inner modes of the perfectly conducting cylinder but also of outer complex modes when the transition coefficient varies from zero to one. In the paper the natural modes are analyzed together with the two-dimensional scattering problem where the cylinder is excited by the H-polarized plane wave. The total and backward scattering cross-sections and the absorption cross-section versus the frequency are presented. It is shown that resonances in the behavior of these cross-sections strongly correlate with the complex frequencies of the natural modes. For a cylinder radius in the micrometer range the principal-mode resonances lay in the THz range. Consequently an important application is sensing at THz frequencies, via measuring the environment-dependent resonance frequencies.

Keywords Circular dielectric cylinder · Graphene layer · Complex frequencies · Total · Backward and absorption cross sections

✉ Alexander Ye. Svezhentsev
oleksandr.svezhentsev@gmail.com

[1] O. Y. Usikov Institute of Radiophysics and Electronics, National Academy of Sciences of Ukraine, Kharkiv 61085, Ukraine

[2] ESAT-WaveCoRE Division, Katholieke Universiteit Leuven, Leuven, Belgium

Published online: 08 January 2023

1 Introduction

Graphene is a very promising material in the THz frequency range because a sheet of graphene supports so-called surface plasmon waves that generate scattering resonances when covering objects (Low and Avouris 2014; Ullah et al. 2020; Fallahi and Perruisseau-Carrier 2012; Hanson 2008). Each resonance of this sort is caused by the corresponding natural mode (eigenmode), the field of which can be viewed as a standing wave created by two oppositely propagating surface waves. Due to the fact that the conductivity of graphene depends on its chemical potential, such structures are extremely attractive as potentially tunable electronic devices. They already find application in chemistry, biosensing, photonics and photodetecting (Rodrigo et al. 2015; Farmani et al. 2020; Zangeneha et al. 2022; Ponnusamy et al. 2022; Seyyedmasoumian et al. 2022; Khosravian et al. 2021). Therefore, the prediction of the electromagnetic behavior of graphene scatterers of various shapes (Christensen et al. 2015; Valencia et al. 2017; Cuevas 2018; Gingins et al. 2020; Svezhentsev et al. 2022) including graphene-covered wires and particles (Zhu et al. 2015; Riso et al. 2015; Velichko 2016; Naserpour et al. 2017; Raad et al. 2019), is important. Moreover, as stated in Dai et al. (2021), micro and nanotubes of graphene, wrapped around circular cylindrical rods of millimeter-scale length, are already fabricated and studied.

The scattering problem of a graphene-covered circular dielectric micro-cylinder (GCCDMC) exited by a plane wave was studied with commercial codes in Zhu et al. (2015), Naserpour et al. (2017), Raad et al. (2019) and a full-wave analytical solution was given in Riso et al. (2015), Velichko (2016). The frequency eigenvalue problem also has been considered with commercial codes (Zhao et al. 2014; Xiao et al. 2015; Zhang et al. 2017), and in Cuevas et al. (2016) an analytical treatment is given for the quasi-static case. A modified eigenvalue problem adapted to the analysis of the lasing modes on the threshold of stationary emission is considered in Herasymova et al. (2022). In this paper the eigen frequencies are real.

In this paper, the complex-frequency eigenvalue problem (CFEP) for a GCCDMC is solved with a full-wave formulation. The spectra of the extinction cross-section (ECS), the absorption cross-section (ACS), and the total cross-section (TSCS), are studied in a wide range, from DC to THz. We demonstrate that the graphene-covered dielectric cylinder is a complicated open resonator, the modes of which form two distinctively different families. One of them is the family of the plasmon modes of the graphene cover on the boundary between the two materials. The other family consists of the modes of the dielectric rod slightly perturbed by the transparent graphene cover. To obtain a clearer vision on the natural modes, we introduce an auxiliary parameter, the transition coefficient, whose variation describes the transformation from a bare dielectric cylinder to a cylinder covered with a perfectly electric conducting (PEC) cover. Using this parameter, we study how the complex modal frequencies migrate in the complex plane versus impedance and dielectric rod permittivity. Mode field patterns are analyzed and compared with scattering resonance patterns. The distinguishing feature of this paper is thus that the plane wave scattering problem (PWSP) analysis is merged with a complex-frequency eigenvalue problem (CFEP) analysis, yielding entirely new insights.

2 Complex frequency eigenvalue problem

The GCCDMC, whose cross-section is shown in Fig. 1, is an infinite dielectric rod of radius r_0, the surface of which is covered with a graphene layer. Two domains, the exterior one (I) and the interior one (II) are introduced. Solving the eigenvalue problem, with no excitation, means determining the complex frequencies $f = \omega/(2\pi)$, where ω is the angular frequency, for which the electromagnetic fields satisfy:

(1) The Helmholtz equation in cylindrical coordinates for the H-polar case in the two domains I and II,
(2) The boundary conditions at the graphene surface $\mathrm{r}=\mathrm{r}_0$,
(3) The radiation condition in domain I,
(4) The condition of local finiteness of power.

The problem can be split into cylindrical modes with azimuthal index n having the dependency $e^{-in\phi}$. Azimuthal degeneration can be circumvented by imposing symmetry with respect to the x-axis. The magnetic field z-components can then be presented as the Helmholtz equation solutions in the two domains as (the assumed time dependence $e^{i\omega t}$ is omitted):

$$H_z^{eig,I}(r_0, z, \phi) = B_n^{eig} H_n^{(2)}(k^I r)\cos(n\varphi) \tag{1}$$

$$H_z^{eig,II}(r_0, z, \phi) = A_n^{eig} J_n(k^{II} r)\cos(n\varphi) \tag{2}$$

where A_n^{eig} and B_n^{eig} are unknown coefficients, $J_n(k^{II}r)$ is the Bessel function, $H_n^{(2)}(k^I r)$ is the Hankel function of the second kind, $k^{(I,II)} = k_0\, n^{(I,II)}$ are the wavenumbers in the two domains, $k_0 = \omega/c = 2\pi f/c$, $n^{(I,II)} = \sqrt{\varepsilon_r^{(I,II)}\mu_r^{(I,II)}}$ is the refractive index, $\varepsilon_r^{(I,II)}$ and $\mu_r^{(I,II)}$ are the relative permittivity and permeability, and k_0 is the free-space wavenumber. In our problem, $\varepsilon_r^I = \mu_r^{(I,II)} = 1$.

The fields in (1)–(2) satisfy the radiation condition and the condition of local finiteness of power. This is achieved by selecting the proper cylindrical function out of the two possible solutions of the Bessel equation. $H_n^{(2)}(k^I r)$ in domain I ensures that the field is an outgoing wave for $r \to \infty$, $J_n(k^{II}r)$ in domain II ensures that the field is finite at $r=0$.

The boundary conditions at the rod surface, $r=r_0$, where the graphene monolayer is located, are the resistive-type boundary conditions derived in Hanson (2008) supplemented with an additional real scalar coefficient, α,

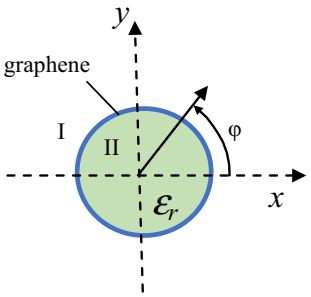

Fig. 1 Cross-sectional view of graphene-covered circular dielectric micro-cylinder with radius $\mathrm{r}=\mathrm{r}_0$

$$\vec{E}_{tg}^{eig,I} + \vec{E}_{tg}^{eig,II} = 2\alpha Z_{grph} Z_0 \vec{n} \times (\vec{H}_{tg}^{eig,I} - \vec{H}_{tg}^{eig,II}), \quad \vec{E}_{tg}^{eig,I} = \vec{E}_{tg}^{eig,II}, \tag{3}$$

where $\vec{n}$ is the outer normal unit vector, Z_0 is the free space surface impedance, and Z_{grph} is the normalized surface impedance of graphene, expressed as (Hanson 2008)

$$Z_{grph} Z_0 = 1/\sigma, \tag{4}$$

where

$$\sigma = \sigma_{\text{intra}} + \sigma_{\text{inter}}, \tag{5}$$

$$\sigma_{\text{intra}} = \frac{\Omega}{i\omega + \tau^{-1}}, \quad \sigma_{\text{inter}} = \frac{-iq_e^2}{4\pi h} \ln \frac{2|\mu_c| - (\omega - i\tau^{-1})h}{2|\mu_c| + (\omega - i\tau^{-1})h}, \tag{6}$$

$$\Omega = \frac{q_e^2 k_B T}{\pi \hbar^2} \left[\frac{\mu_c}{k_B T} + 2 \ln \left(1 + \exp(-\frac{\mu_c}{k_B T}) \right) \right], \tag{7}$$

where μ_c is the chemical potential, h is the reduced Planck constant, τ is the electron relaxation time, q_e is the electron charge, and T is the absolute temperature. The coefficient α is introduced to collect the graphene case ($\alpha = 1$), the PEC case ($\alpha = 0$), and the dielectric boundary condition case ($\alpha \to \infty$) in a single unified formulation. The intermediate α values do not have any truly physical sense. However, this parameter allows tracing the mode transformation from the graphene-coated cylinder to the PEC and the dielectric cylinder cases.

The Poynting Theorem results in the fact that the natural frequencies of an open resonator can be only complex because of the radiation losses. Note that due to the Hankel function the complex frequency definition area represents multi sheet logarithmic Riemann surface with the single branching point at $k_0 = 0$. In this paper, we find complex eigenfrequencies that are localized on the principal (physical) sheet of this surface. To define this sheet, we arrange a cut on the complex frequency plane from zero to infinity that runs, for definiteness, along the negative part of the real axis.

Applying the condition (3) at the graphene surface, we obtain

$$\begin{bmatrix} a_{11} & a_{12} \\ a_{21} & a_{22} \end{bmatrix} \begin{bmatrix} A_n^{eig} \\ B_n^{eig} \end{bmatrix} = 0 \tag{8}$$

where

$$a_{11} = J_n'(\chi^{II} r_0)/n^{II} + 2i(\alpha Z_{grph} Z_0) J_n(\chi^{II} r_0), \; a_{12} = H_n^{(2)'}(\chi^I r_0)/n^I - 2i(\alpha Z_{grph} Z_0) H_n(\chi^I r_0), \tag{9}$$

$$a_{21} = J_n'(\chi^{II} r_0)/n^{II}, \; a_{22} = -H_n^{(2)'}(\chi^I r_0)/n^I, \; \chi^I = k^I r_0, \; \chi^{II} = k^{II} r_0 \tag{10}$$

A solution exists only if the determinant of the matrix in (8) is zero:

$$\Delta_n = 0, \tag{11}$$

where

$$\begin{aligned}\Delta_n = &-\left[J_n'(\chi^{II}r_0)/n^{II} + 2i(\alpha Z_{grph}Z_0)J_n(\chi^{II}r_0)\right]H_n^{(2)'}(\chi^{I}r_0)/n^{I} \\ &-\left[H_n^{(2)'}(\chi^{I}r_0)/n^{I} - 2i(\alpha Z_{grph}Z_0)H_n(\chi^{I}r_0)\right]J_n'(\chi^{II}r_0)/n^{II}\end{aligned} \tag{12}$$

The expression (12) is called the characteristic equation for the natural complex frequencies, $f = f^{eig}$. This equation can be solved using Newton's method. Once a natural frequency is known, its natural modal field is easily calculated.

It is known that a graphene layer supports surface waves which "cling" to its surface (Hanson 2008). This leads to the fact that the structural spectrum consists of two types of eigenmodes. The first type consists of graphene modes, modified by the presence of the dielectric rod. These modes are the so-called plasmonic modes, P_n. The second type consists of the GH_{nm} modes of the dielectric rod, modified by the presence of the graphene layer. Note that the transversal modes of a circular dielectric rod split into so-called internal and external modes (Herasymova et al. 2022).

It is easily shown from (10)–(11) that in the case of $\alpha=0$ (PEC cylinder at $r=r_0$) the natural modes split into two families, satisfying the following characteristic equations:

$$J_n'(k^{II}r_0) = 0 \quad (H_{mn}^{PEC,IN}\text{modes}), \tag{13}$$

$$H_n^{(2)'}(k^{I}r_0) = 0 \quad (H_{nm}^{PEC,OUT}\text{modes}), \tag{14}$$

where m corresponds to the variation along r. Real solutions of (13) and complex solutions of (14) are known and can be found in Dettmann et al. (2009).

In the following sections it is demonstrated that the $H_{mn}^{PEC,IN}$ and $H_{nm}^{PEC,OUT}$ modes of the PEC cylinder transform into the P_n and perturbed GH_{nm} modes if the parameter α varies from 0 (the PEC cylinder case) to 1 (the graphene case). If $\alpha \to \infty$, then the plasmon mode eigenfrequencies move to $k_0=0$ and disappear while the dielectric rod mode eigenfrequencies survive.

3 H-polarized plane wave scattering problem

The problem geometry is shown in Fig. 2 where the GCCDMC is excited by an H-polarized plane wave incident along the –x direction. The incident magnetic field is in the z-direction and given by

$$\mathrm{H}_z^{inc} = \mathrm{H}^0 \exp(ik_0 x) \tag{15}$$

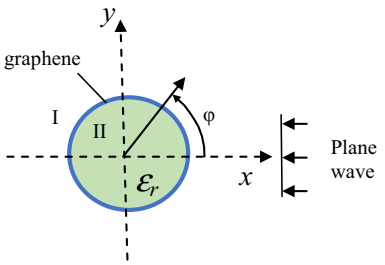

Fig. 2 Cross-sectional view of graphene-covered circular dielectric micro-cylinder with radius $r=r_0$, excited by a plane wave

The full-wave formulation of the scattering problem involves the Helmholtz equations in regions I and II, the boundary conditions on the cylinder surface, the radiation condition at infinity, and the condition of local power finiteness.

In domains I and II, the total z-directed magnetic field components are expressed as Fourier series in the azimuthal coordinate. Each term in the series satisfies the Helmholtz equation. Taking into account the structure and the excitation field symmetry with respect to $y=0$, the result is:

$$H_z^{tot,I}(r,z,\varphi) = H_z^{inc}(r,z,\varphi) + H_z^{sc,J}(r,z,\phi) = \sum_{n=0}^{\infty} \delta_n \left[i^n J_n(k^I r) + B_n H_n^{(2)}(k^I r) \right] \cos(n\varphi) \tag{16}$$

$$H_z^{tot,II}(r_0,z,\varphi) = H_z^{sc,II}(r,z,\varphi) = \sum_{n=0}^{\infty} \delta_n A_n J_n(k^{II} r)\ \cos(n\varphi), \tag{17}$$

where A_n and B_n are unknown coefficients, the indices "scat" and "tot" stand for the scattered and the total field, respectively, δ_n is 1 if $n=0$ and 2, otherwise. The scattered field satisfies the radiation condition in the domain I and the condition of local finiteness of energy in domain II (see also the previous section).

To find the unknown coefficients, the same resistive-type boundary conditions as in (3) need to be satisfied

$$\vec{E}_{tg}^{tot,I} + \vec{E}_{tg}^{tot,II} = 2\alpha Z_{grph} Z_0 \vec{n} \times (\vec{H}_{tg}^{tot,I} - \vec{H}_{tg}^{tot,II}), \quad \vec{E}_{tg}^{tot,I} = \vec{E}_{tg}^{tot,II}, \tag{18}$$

at $r=r_0$ where the graphene monolayer is located.

Using (18) for each azimuthal index value, $n=0, 1, 2, \ldots$, a 2×2 matrix equation for the unknown coefficients A_n and B_n is obtained,

$$\begin{bmatrix} a_{11} & a_{12} \\ a_{21} & a_{22} \end{bmatrix} \begin{bmatrix} A_n \\ B_n \end{bmatrix} = \begin{bmatrix} b_1 \\ b_2 \end{bmatrix} \tag{19}$$

with the solution

$$A_n = (b_1 a_{22} - b_2 a_{12})/\Delta_n, \tag{20}$$

$$B_n = (-b_1 a_{21} + b_2 a_{11})/\Delta_n, \tag{21}$$

where

$$b_1 = -i^n J_n'(\chi^I r_0)/n^{II} + 2i^{n+1}(\alpha Z_{grph} Z_0) J_n(\chi^I r_0),\ b_2 = i^n J_n'(\chi^I r_0) \tag{22}$$

For $\alpha \to 0$ the case with a PEC cover at $r=r_0$ is obtained. In this case only in domain I a non-zero field exists.

The total scattering cross section (TSCS) is

$$\sigma_{tscs} = \frac{4}{k_0} \sum_{n=0}^{\infty} \delta_n \left| B_n \right|^2, \tag{23}$$

the extinction cross section (ECS) is

$$\sigma_{ecs} = \frac{4}{k_0}\mathrm{Re}\sum_{n=0}^{\infty}\delta_n\,(-i)^n B_n \tag{24}$$

and the absorption cross section (ACS), which can be found from the optical theorem (power conservation law), is

$$\sigma_{acs} = \sigma_{ecs} - \sigma_{tscs} \tag{25}$$

Note that the left-hand part of the characteristic Eq. (11) is present in the denominators of the field expansion coefficients (20) and (21). Therefore, the complex natural frequencies discussed in the previous section will occur as resonances of TSCS, ECS and ACS.

4 Numerical results

First, the evolution of the complex eigenfrequencies versus the parameter α is discussed. In Fig. 3 the real and imaginary parts of the complex eigenfrequencies f_{nm}^{eig} are plotted for α varying from 0 (the PEC case) to 1 (the graphene case). The modes $H_{nm}^{PEC,(IN,OUT)}$ exist at $\alpha = 0$ and transform to the plasmon modes P_n and the dielectric-rod modes $GH_{n\,m}$. It is interesting to note that in the interior domain (Im $f_{nm}^{eig}=0$) only the H_{11}^{IN} mode transforms to the plasmon mode P_1. All other modes in the interior domain transform to modes of the the $GH_{n\,m}$ type, except the GH_{11} mode. The modes in the exterior domain transform to P_n modes.

It is seen from Fig. 3a that if α increases, the real parts of f_{nm}^{eig} for the family `PEC,IN` ($\alpha=0$) decrease while for the family `PEC,OUT` they display a small change. In Fig. 3b, there is a clearer situation for the imaginary parts of f_{nm}^{eig}, namely, for the family `PEC,IN` there is an increase starting from 0. This is because for $\alpha=0$ the inner family modes have real eigenfrequencies while for the outer family modes the eigenfrequencies are complex with large imaginary parts. It follows from Fig. 3 that, in general, the modes are strongly affected by the graphene presence. Note that for the majority of the modes of the family `PEC,OUT` the imaginary parts decrease if α increases, and finally at $\alpha=1$ (the graphene case) these modes have smaller losses than the lowest `PEC,IN` modes. This means that when the graphene replaces the PEC screen, the modal fields of the `PEC,IN` family radiate out of the cylinder $r=r_0$ and, on the contrary, the mode fields of the `PEC,OUT`

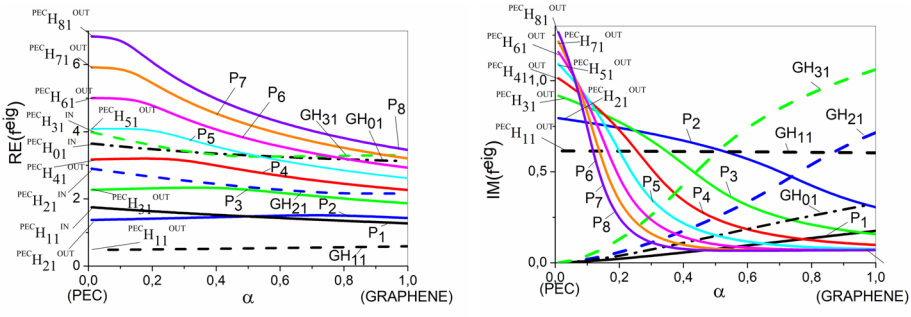

Fig. 3 Real (**a**) and imaginary (**b**) parts of the complex eigenfrequencies f^{eig} versus α. $r_0=50$ μm, $\varepsilon^{II}=1$. $\alpha = 0$ corresponds to the PEC cylinder and $\alpha = 1$ to the graphene shell in free space

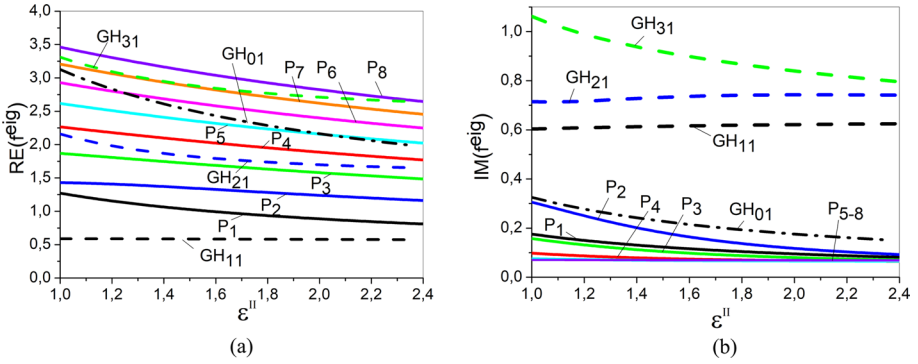

Fig. 4 Real (**a**) and imaginary (**b**) parts of the complex eigenfrequencies f^{eig} versus ε_r^{II} at $\alpha = 1$ (the graphene case) and $r_0 = 50$ μm

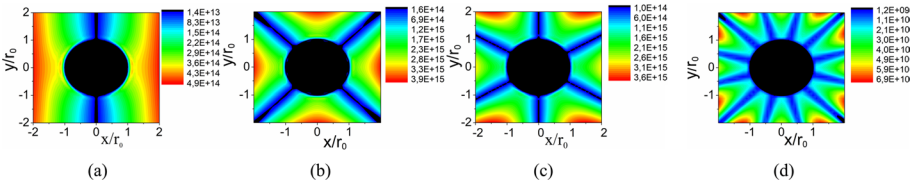

Fig. 5 Absolute value of the H_z component for the outer family eigenmodes for the PEC cylinder ($\alpha = 0$) with $r_0 = 50$ μm: **a** $H_{11}^{PEC,OUT}$, $f^{eig} = 0.4786 + i\ 0.6145$; **b** $H_{21}^{PEC,OUT}$, $f^{eig} = 1.3717 + i0.7944$, **c** $H_{31}^{PEC,OUT}$, $f^{eig} = 2.2668 + i0.9239$; **d** $H_{61}^{PEC,OUT}$, $f^{eig} = 5.0001 + i1.15775$. All frequencies are given in THz

family penetrate into this cylinder. It is interesting to observe that the $H_{11}^{PEC,OUT}$ mode is only slightly affected by the α parameter. Both the real and imaginary parts of its eigenfrequency demonstrate small changes.

Next, we discuss the GCCDMC eigenmodes transformation versus the dielectric rod permittivity,ε_r^{II}, from $\varepsilon_r^{II} = 1$ to $\varepsilon_r^{II} = 2.4$ assuming that $\alpha = 1$. This transformation is presented for the real and imaginary parts of the eigenfrequencies f^{eig}, respectively, in Fig. 4a, b. It is seen from Fig. 4a that the real parts of the eigenfrequencies decrease for all presented modes except for GH_{11}. For this mode the real part of the eigenfrequency stays almost unchanged. For the imaginary parts (see Fig. 4b), for all modes the situation is similar, except for the GH_{11} and GH_{21} modes. It is observed here that the plasmon modes P_n are more affected by the parameter ε_r^{II} than the $GH_{n\,m}$ modes.

Below, the eigenmode field patterns are illustrated, by presenting the amplitude of the H_z component over the structure cross-section in the case of the PEC cylinder, see Fig. 5a, b for the outer modes of the "PEC,OUT" family: $H_{11}^{PEC,OUT}$, $H_{21}^{PEC,OUT}$, $H_{31}^{PEC,OUT}$, $H_{61}^{PEC,OUT}$, respectively.

It is easily seen that the field grows with r. This means that the PEC cylinder does not hold the field, but it leaks away from the structure. This is a typical feature of an open resonator, and in this case it corresponds to the asymptotical behavior of the Hankel function, $H_n^{(2)}(k^I r)$ (see (1)), taking into account that the eigenfrequency has a positive imaginary part. Hence, in the Complex Field Eigenvalue Problem (CFEP) the modal field always decays with time t and grows with distance r.

For the graphene case, in the outer region ($r > r_0$) the modal field patterns behave in similar manner. However, in the inner domain and at $r = r_0$ different modal families behave differently (see Fig. 6).

It is seen that the modes of the plasmon family, P_n, have fields concentrated only close to the graphene layer, while the modes of the $GH_{n\,n}$ family show variations in the r direction. Such a difference is clearly visible for the modes with $n = 1$, namely, GH_{11} and P_1. Based on the comparison of the eigenfrequency imaginary parts, it can be stated that the Q factor of the P_1 mode is considerably larger than the one for the GH_{11} mode.

Now the results of the PWSP and CFEP problems will be combined. To begin with, consider the 50 μm radius PEC cylinder. Its normalized TSCS versus frequency is shown in Fig. 7, together with the complex eigenfrequencies (stars). This plot does not show any resonance behavior at all. This is because the Q factors of the $H_{mn}^{PEC,OUT}$ modes with $m = 1$ to 6 are very low, lower than 2.

The TSCS, ECS, and ACS (all normalized by $4r_0$) versus frequency are presented in Figs. 8 and 9, for $\varepsilon_r^{II} = 1$ and $\varepsilon_r^{II} = 2.4$, respectively. Together with these cross-sections, the complex eigenfrequencies of the natural modes are depicted by stars. It is seen that in the

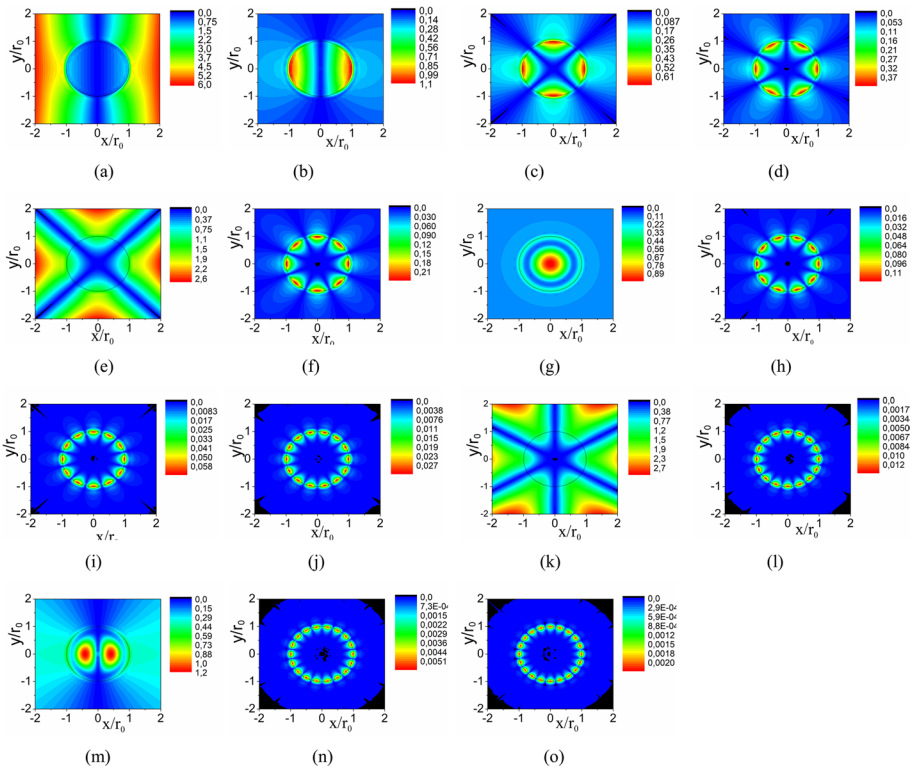

Fig. 6 Amplitude of H_z component for complex eigenmodes of the graphene cylinder ($\alpha = 1$) with dielectric filling $\varepsilon^{II} = 2.4$, $\mu_c = 0.5$ eV, $T = 300$ K, and $\tau = 10^{-12}$ s., $r_0 = 50$ μm: **a**—GH_{11}, $f^{eig} = 0.5738 + i0.6247$, **b**—$P_1$, $f^{eig} = 0.8094 + i0.08124$, **c**—$P_2$, $f^{eig} = 1.1616 + i0.09246$, **d**—$P_3$, $f^{eig} = 1.4844 + i0.07036$, **e**—$GH_{21}$, $f^{eig} = 1.6472 + i0.7412$, **f**—$P_4$, $f^{eig} = 1.7712 + i0.06459$, **g**—$DH_{01}$, $f^{eig} = 1.9698 + i0.1491$, **h**—$P_5$, $f^{eig} = 2.0232 + i0.06514$, **i**—$P_6$, $f^{eig} = 2.2490 + i0.06686$, **j**—$P_7$, $f^{eig} = 2.4553 + i0.06842$, **k**—$GH_{31}$, $f^{eig} = 2.6374 + i0.7955$, **l**—$P_8$, $f^{eig} = 2.6463 + i0.06967$, **m**—$GH_{12}$, $f^{eig} = 2.7923 + i0.2306$, **n**—$P_9$, $f^{eig} = 2.825 + i0.0706$, **o**—$P_{10}$, $f^{eig} = 2.993 + i0.0714$. All frequencies are given in THz

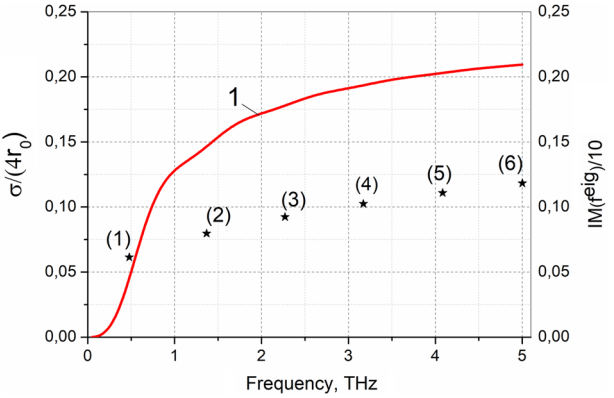

Fig. 7 Normalized scattering cross-section versus frequency for the PEC circular cylinder ($\alpha = 0$) with $r_0 = 50$ μm (curve 1). The stars correspond to the complex eigenfrequencies: (1) for $H_{11}^{PEC,OUT}$, (2) for $H_{21}^{PEC,OUT}$, (3) for $H_{31}^{PEC,OUT}$, (4) for $H_{41}^{PEC,OUT}$, (5) for $H_{51}^{e,OUT}$, (6) for $H_{61}^{e,OUT}$

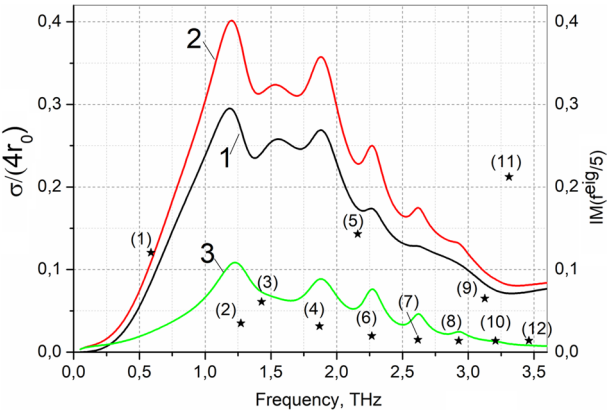

Fig. 8 Normalized scattering and absorption cross-sections versus frequency for the circular graphene shell ($\alpha = 1$) in free space ($\varepsilon_r^{II} = 1$): TSCS is marked 1, ECS is marked 2, and ACS is marked 3. The graphene parameters are $\mu_c = 0.5$ eV, $T = 300$ K, and $\tau = 10^{-12}$ s, $r_0 = 50$ μm. Stars denote the complex natural frequencies: (1) for GH_{11}, (2) for P_1, (3) for P_2, (4) for P_3, (5) for GH_{21}, (6) for P_4, (7) for P_5, (8) for P_6, (9) for GH_{01}, (10) for P_7, (11) for GH_{31}, (12) for P_8

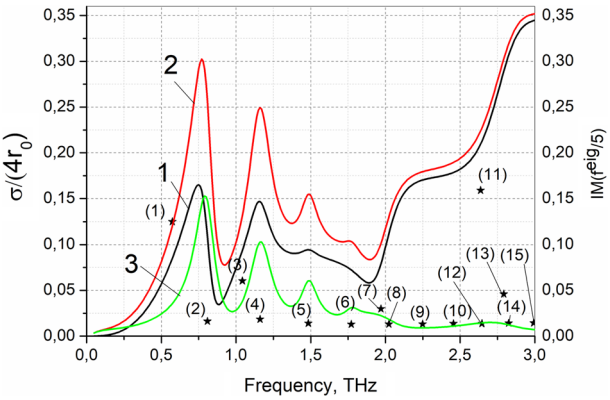

Fig. 9 Normalized scattering, extinction and absorption cross-sections versus frequency for GCCDMC ($\alpha = 1$, $\varepsilon_r^{II} = 2.4$): TSCS is marked 1, ECS is marked 2, and ACS is marked 3. The rod and graphene parameters are $r_0 = 50$ μm, $\mu_c = 0.5$ eV, $T = 300$ K, and $\tau = 10^{-12}$ s, $r_0 = 50$ μm. Stars denote the complex eigenfrequencies: (1) for GH_{11}, (2) for P_1, (3) for P_2, (4) for P_3, (5) for GH_{21}, (6) for P_4. (7) for GH_{01}, (8) for P_5, (9) for P_6, (10) for P_7, (11) for GH_{31}, (12) for P_8, (13) for GH_{12}, (14) for P_9, (15) for P_{10}

case $\varepsilon_r^{II}=1$ (Fig. 8) all resonant frequencies correlate well with the plasmon modes, P_n. Modes like GH_{11}, GH_{21}, GH_{01} and DH_{31}, whose complex frequencies have large imaginary parts and hence low Q-factors, do not produce any visible resonance effects. In the case of $\varepsilon_r^{II}=2.4$ (see Fig. 9), the mode GH_{12} appears in the higher part of the studied frequency band. However, it does not show up as a peak on the plots of the cross-sections, because of a similarly low Q-factor.

Comparison of Figs. 8 and 9 shows that the dielectric with $\varepsilon_r^{II}=2.4$ in the inner domain influences the real parts of the plasmon mode frequencies in such a way that they are down-shifted. The Q-factors are somewhat lowered, although not dramatically.

Note that in the case of the graphene boundary, the degree of transparency of that boundary depends on the graphene's surface impedance: the lower the impedance, the lower the transparency (i.e. the closer the cover to the PEC case). Here, one must take into account that the graphene's impedance depends on the frequency according to Eqs. (5)–(8) and its imaginary part goes to zero if the frequency goes to zero. As a result, at frequencies lower than approximately 3 THz (if the graphene's chemical potential is 1 eV), the graphene cover is highly conducting and all lower-order outer modes of the PEC cylinder, now slightly perturbed by the imperfect conductivity of graphene, are present. Still, they do not result in any pronounced resonances in the TSCS and ACS spectra because of the very low Q-factors, caused by the graphene losses.

At frequencies higher than approximately 3 THz, the graphene's conductivity tends to be low, and it becomes well transparent. In this range, the natural modes of the GCCDMC are close to the modes of the bare dielectric circular cylinder, with the "inner" and "outer" mode families (Herasymova et al. 2022). Note that there exists a one-to-one correspondence between these modes and the modes of the inner and outer domains of the PEC cylinder. This can be clearly demonstrated by an analysis of the effect of the parameter α varying from 1 to infinity.

Still, the presence of the graphene cover ($\alpha = 1$) yields new natural modes, absent in two limiting cases: the PEC cover ($\alpha = 0$) and the dielectric rod ($\alpha = \infty$). These new modes are the plasmon modes. The real part of their lowest eigenfrequency with azimuth index 1 lays in the sub-THz range for the 50 μm radius cylinder. The Q-factors of the plasmon modes are an order of magnitude larger than the ones of the "outer" modes. Therefore the associated resonance peaks are well visible in the spectra of the TSCS and ACS in the range below approximately 3 THz.

5 Conclusions

The plane-wave scattering problem and the complex-frequency eigenvalue problem of a GCCDMC excited by an H-polarized plane wave have been studied. As a reference, the simple case of a hollow PEC circular cylinder was considered. For the GCCDMC frequency eigenvalue problem it has been shown that the spectrum consists of two families: the plasmon modes, the fields of which are compressed to the graphene cover, and the modes of the dielectric rod perturbed by the graphene cover. Moreover, we have introduced an auxiliary coefficient. If this coefficient varies from 0 to 1, then its product with the impedance varies from the PEC to the graphene case. This coefficient was proven to be very efficient when studying the transformation of the modes from one case to another. It was proven that the plasmon modes are related to both the "PEC, IN" family (modes existing only inside the PEC cylinder) and the "PEC, OUT" family (modes existing only

outside the PEC cylinder). However, the plasmon modes are singular because they do not exist in the PEC limiting case. If the auxiliary coefficient grows larger than 1 and even goes to infinity (not presented here), the other limiting case is realized—the bare dielectric rod, which does not have plasmon natural modes at all. It was also shown that for a 50 μm radius dielectric rod the first five plasmon-mode resonances, since they have the highest Q factors, can be easily identified as the peaks on the cross-section plots. Higher modes have a lower Q factor and do not produce any visible resonances.

Acknowledgements Alexander Nosich and Alexander Svezhentsev are grateful to the Universite de Rennes 1, the Politechnico di Torino, and KU Leuven, respectively, for the hospitality via the programs of solidarity with Ukraine. Also, they both are grateful to the IOP Physics Benevolent Fund for the one-off emergency support.

Authors contribution AYS conceived of the presented idea, developed the numerical algorithm, performed computations, prepared Figures and sections II and III. AIN prepared the abstract, introduction, conclusions, and references and contributed to the article physical interpretation. VV reviewed the obtained results. GAEV updated the whole manuscript. All authors discussed the results and contributed to the final manuscript.

Funding This work was supported, in part, by the National Academy of Sciences of Ukraine via project #6541230-0204-2022.

Data availability The authors present, in the paper, all relevant equations, which are easily programmed in direct manner and lead to the computer code that delivers all the presented results.

Declarations

Conflict of interest The authors have no competing interests.

References

Christensen, T., Jauho, A., Wubs, M., Mortensen, N.A.: Localized plasmons in graphene coated nanospheres. Phys. Rev. B **91**, 125414 (2015)

Cuevas, M.: Spontaneous emission in plasmonic graphene subwavelength wires of arbitrary sections. J. Quant. Spectrosc. Radiat. Transf. **206**, 157–162 (2018)

Cuevas, M., Riso, M.A., Depine, R.A.: Complex frequencies and field distributions of localized surface plasmon modes in graphene-coated subwavelength wires. J. Quant. Spectrosc. Radiat. Transf. **173**, 26–33 (2016)

Dai, C., Agarwal, K., Bechtel, H.A., Liu, C., Joung, D., Nemilentsau, A., Su, Q., Low, T., Koester, S.J., Cho, J.-H.: Hybridized radial and edge coupled 3D plasmon modes in self-assembled graphene nanocylinders. Small **17**, 2100079 (2021)

Dettmann, C.P., Morozov, G.V., Sieber, M., Waalkens, H.: Internal and external resonances of dielectric disks. Eur. Phys. Lett. **87**, 34003 (2009)

Fallahi, A., Perruisseau-Carrier, J.: Design of tunable biperiodic graphene metasurfaces. Phys. Rev. B **86**, 195408 (2012)

Farmani, H., Farmani, A., Biglari, Z.: A label-free graphene-based nanosensor using surface plasmon resonance for biomaterials detection. Phys. E Low Dimens. Syst. Nanostruct. **116**, 113730 (2020)

Gingins, M., Cuevas, M., Depine, R.: Surface plasmon dispersion engineering for optimizing scattering, emission, and radiation properties on a graphene spherical device. Appl. Opt. **59**(14), 4254–4262 (2020)

Hanson, G.W.: Dyadic Green's functions and guided surface waves for a surface conductivity model of graphene. J. Appl. Phys. **103**, 064302 (2008)

Herasymova, D.O., Natarov, D.M., Dukhopelnykov, S.V., Zinenko, T.L., Lucido, M., Nosich, A.I.: Threshold conditions for transversal modes of tunable plasmonic nanolasers shaped as single and twin graphene-covered circular quantum wires. IOP Nanotechnology **34**, 495001 (2022). https://doi.org/10.1088/1361-6528/ac8e0c

Khosravian, E., Mashayekhi, H.R., Farmani, A.: Highly polarization-sensitive, broadband, low dark current, high responsivity graphene-based photodetector utilizing a metal nano-grating at telecommunication wavelengths. J. Opt. Soc. Am. B **38**(4), 1192–1199 (2021)

Low, T., Avouris, P.: Graphene plasmonics for terahertz to mid-infrared applications. ACS Nano **8**, 1086–1101 (2014)

Naserpour, M., Zapata-Rodríguez, C.J., Vuković, S.M., Pashaeiadl, H., Belić, M.R.: Tunable invisibility cloaking by using isolated graphene-coated nanowires and dimers. Sci. Rep. **7**(1), 1–14 (2017)

Ponnusamy, M., Ramya, K.C., Sivasankaran, V., Farmani, H., Farmani, A.: Emerging advanced photonics applications of graphene and beyond-graphene 2D materials: recent advances. J. Mater. Res. **37**, 391–404 (2022)

Raad, S.H., Zapata-Rodríguez, C.J., Atlasbaf, Z.: Multi-frequency super-scattering from subwavelength graphene-coated nanotubes. J. Opt. Soc. Am. B **36**(8), 2292–2298 (2019)

Riso, M., Cuevas, M., Depine, R.A.: Tunable plasmonic enhancement of light scattering and absorption in graphene coated subwavelength wires. J. Opt. **17**, 075001 (2015)

Rodrigo, D., Limaj, O., Janner, D., Etezadi, D., García de Abajo, F.J., Pruneri, V., Altug, H.: Mid-infrared plasmonic biosensing with graphene. Science **349**(6244), 165–168 (2015)

Seyyedmasoumian, S., Attariabad, A., Farmani, A.: FEM analysis of a $\lambda^3/125$ high sensitivity graphene plasmonic biosensor for low hemoglobin concentration detection". Appl. Opt. **61**(1), 120–125 (2022)

Svezhentsev, A.Y., Dukhopelnykov, S.V., Volski, V., Vandenbosch, G.A.E., Nosich, A.I.: Microsized graphene Helmholtz resonator on circular dielectric rod: a tunable sub-THz frequency-selective scatterer. IEEE Trans. Antennas Propag. **70**(3), 2105–2113 (2022)

Ullah, Z., Witjaksono, G., Nawi, I., Tansu, N., Khattak, M.I., Junaid, M.: A review on the development of tunable graphene nanoantennas for terahertz optoelectronic and plasmonic applications. Sensors **20**(5), 1401 (2020)

Valencia, C., Riso, M.A., Cuevas, M., Depine, R.A.: Green formulation for studying electromagnetic scattering from graphene-coated wires of arbitrary section. J. Opt. Soc. Am. B **34**(6), 1075–1083 (2017)

Velichko, E.A.: Evaluation of a dielectric microtube with a graphene cover as a refractive-index sensor in the THz range. J. Opt. **18**(3), 035008 (2016)

Xiao, T.-H., Gan, L., Li, Z.-Y.: Graphene surface plasmon polaritons transport on curved substrates. Photon. Res. **3**, 300–307 (2015)

Zangeneh, A.M.R., Farmani, A., Mozaffari, M.H., Mir, A.: Enhanced sensing of terahertz surface plasmon polaritons in graphene/J-aggregate coupler using FDTD method. Diam. Relat. Mater. **125**, 109005 (2022)

Zhang, W., Wu, T., Zhang, X.: Tailoring eigenmodes at spectral singularities in graphene-based PT systems. Sci. Rep. **7**, 11407 (2017)

Zhao, J., Liu, X., Qiu, W., Ma, Y., Huang, Y., Wang, J.-X., Qiang, K., Pan, J.-Q.: Surface-plasmon-polariton whispering-gallery mode analysis of the graphene monolayer coated InGaAs nanowire cavity. Opt. Express **22**(5), 5754–5761 (2014)

Zhu, B., Ren, G., Yang, Y., Gao, Y., Wu, B., Lian, Y., Wang, J.: Field enhancement and gradient force in the graphene-coated nanowire pairs. Plasmonics **10**(4), 839–845 (2015)

Publisher's Note Springer Nature remains neutral with regard to jurisdictional claims in published maps and institutional affiliations.

Springer Nature or its licensor (e.g. a society or other partner) holds exclusive rights to this article under a publishing agreement with the author(s) or other rightsholder(s); author self-archiving of the accepted manuscript version of this article is solely governed by the terms of such publishing agreement and applicable law.